EUROPEAN ORGANISATION FOR NUCLEAR RESEARCH (CERN)

6th October, 2016
Revision: 31st October, 2016

Expected Performance of the ATLAS Inner Tracker at the High-Luminosity LHC

The ATLAS Collaboration

Abstract

The large data samples at the High-Luminosity LHC will enable precise measurements of the Higgs boson and other Standard Model particles, as well as searches for new phenomena such as supersymmetry and extra dimensions. To cope with the difficult challenges such as large radiation doses and high pileup, during Phase II of the ATLAS upgrade the current Inner Detector will be replaced with a new all-silicon Inner Tracker. The current tracking performance of two candidate Inner Tracker layouts with a wide acceptance of $|\eta| < 4.0$, employing either an Extended or Inclined Pixel barrel, is evaluated. The forward coverage would enable track-based rejection of forward pileup jets, which is particularly beneficial for studies of vector boson scattering and Higgs boson production through vector boson fusion.

Table 2 has been updated to correct a typographical error: the maximum $|z|$ position of the modules in Pixel endcap layer 1 is 3000 mm, not 2596 mm.

ATL-PHYS-PUB-2016-025
31/10/2016

Contents

1. Introduction

1.1. High-Luminosity LHC

The Large Hadron Collider (LHC) currently collides protons at a center-of-mass energy of 13 TeV, with a design energy of 14 TeV. The High-Luminosity LHC (HL-LHC), which will also operate at 14 TeV, is at present expected to begin operation in the second half of 2026 [1]. It was expected to achieve a nominal levelled instantaneous luminosity of $\mathcal{L} = 5\times10^{34}$ cm^{-2}s^{-1} corresponding roughly to an average $\langle\mu\rangle$=140 inelastic pp collisions per beam-crossing and deliver an integrated luminosity of around 250 fb^{-1} per year of operation. The ATLAS Collaboration has described its initial plan and goals for the corresponding Phase-II upgrade of the detector, intended to take full advantage of this accelerator upgrade, in the Letter of Intent (LoI) [2] in 2012.

More recently the target ultimate luminosity has been updated to 7.5×10^{34} cm^{-2}s^{-1}, corresponding to an average $\langle\mu\rangle$ =200 inelastic pp collisions per beam-crossing. This programme aims to provide a total

integrated luminosity of 3000 fb^{-1} by 2035. The refinement and improvement of the Phase-II detector upgrade plans since the LoI are described in the Scoping Document [3].

1.2. Physics motivation

The physics programme of the LHC luminosity upgrade is presented and discussed in detail in the Scoping Document [3], Phase-II Upgrade LoI [2], and in the two reports submitted to the European Committee for Future Accelerators (ECFA) [4, 5]. The benchmark physics analyses for the Phase-II program focus primarily on precision measurements of the 125 GeV Higgs boson [6, 7], on vector-boson scattering [8], and on searches for signatures of new physics such as supersymmetric particles [9] and extra dimensions [3].

One of the strongest motivations for a tracker with coverage out to pseudorapidity[1] $|\eta| = 4.0$ is the ability to reject forward pileup jets by associating the signal jets to the hard-scattering vertex using tracks. Measurements of vector boson fusion (VBF) production of Higgs bosons are important to precisely test the Higgs boson couplings. This process is selected using forward jets that preferentially populate the region $|\eta| > 2.5$. Study of vector boson scattering (VBS) is important to establish whether other mechanisms besides the 125 GeV Higgs boson are responsible for unitarity in this process. VBS processes are also characterised by high-p_{T} forward jets.

1.3. ATLAS Tracker Upgrade

The current ATLAS Inner Detector will have reached the end of its lifetime by 2026. It will not be able to cope with the very high pile-up, radiation doses, occupancies, and data transmission rates at the HL-LHC. Thus it will be replaced with an all-silicon Inner Tracker (ITk), which is outlined in Section 2. The basic components of the ITk detector are described in more detail in the Letter of Intent [2]. The other planned upgrades to the ATLAS detector are discussed in the Scoping Document [3].

1.4. Outline

An overview of the ITk and the different potential tracker layouts being evaluated is given in Section 2. The simulation of the detector in different pileup conditions is described in Section 3. The track reconstruction is detailed in Section 4, and the tracking performance is discussed in Section 5. Finally, Section 6 is devoted to the conclusions.

[1] ATLAS uses a right-handed coordinate system with its origin at the nominal interaction point in the centre of the detector and the z-axis along the beam pipe. The x-axis points from the interaction point to the centre of the LHC ring and the y-axis points upward. Cylindrical coordinates (r, ϕ) are used in the transverse plane, ϕ being the azimuthal angle around the beam pipe. The pseudorapidity is defined in terms of the polar angle θ as $\eta = -\ln\tan\left(\frac{\theta}{2}\right)$.

2. ATLAS Phase II Tracker

2.1. Inner Tracker (ITk)

The ITk for the Phase-II upgrade of ATLAS is an all-silicon tracker consisting of Pixel and Strip detectors [2, 3]. It is being designed to yield at least 13 clusters per charged particle in the central region, as well as to provide uniform coverage in the forward region where the design requirements are still evolving. This would allow the ITk to precisely measure the transverse momenta and directions of isolated particles (in particular muons and electrons), to reconstruct and resolve vertices from the collisions, and to identify the vertex originating from the hardest interaction. The momentum measurement is to be carried out using the same 2 Tesla solenoidal magnetic field as the current Inner Detector. The new Inner Tracker should be able to identify secondary vertices in b-jets with high efficiency and low fake rate, measure the tracks in the cores of high energy jets with high efficiency, provide good two-track resolution, and ensure a low probability to falsely reconstruct a track in absence of a real particle. It should also identify the decay of τ leptons, including impact parameter information, and reconstruct the vertices and tracks associated with converted photons.

Figure 1 shows two candidate ITk layouts, referred to as "Extended" and "Inclined" depending on the design of the Pixel tracker, that are under evaluation. In both scenarios, the Pixel tracker covers the pseudorapidity region up to $|\eta| = 4.0$. This would provide tracking and vertexing capabilities in the forward region, and thereby enable to reject forward pileup jets, whose tracks mostly originate from pileup vertices rather than from the hard-scatter vertex.

The current layouts studied differ with respect to the "LoI" (Letter of Intent) layout [2] as follows:

- The Pixel system has been modified to cover a wider pseudorapidity region, $|\eta| < 4.0$.
- The number of Pixel barrel layers has been increased from 4 to 5.
- The Pixel endcap system now uses four rings of different size, instead of discs, which are arranged to provide uniform coverage in terms of number of clusters as a function of η.
- The number of Strip double-sided barrel layers has been decreased from 5 to 4.
- The Strip barrel has been significantly lengthened, and the number of Strip endcap discs has been reduced from 7 to 6.
- The Strip "stub" layer, which is a very short layer that covers a small gap between the Strip barrel and endcap in the approximate region $1.0 < |\eta| < 1.2$, has been removed.

2.2. Pixel barrel layouts

The two ITk layouts studied differ in the structural design used for the Pixel barrel. The Pixel endcaps and the Strip tracker are identical for the two layouts. Figure 2 shows zoomed-in views of the Pixel tracker in these two layouts.

The "Extended" layout has a Pixel barrel where the innermost layer covers the full range of pseudorapidity $|\eta| < 4.0$, along with a second elongated inner barrel layer and a shorter 3-layer outer barrel. In the very forward region, the two long innermost layers of the Extended layout produce very long clusters spanning many pixels due to the shallow incident angle, with a long path length through the silicon. The cluster

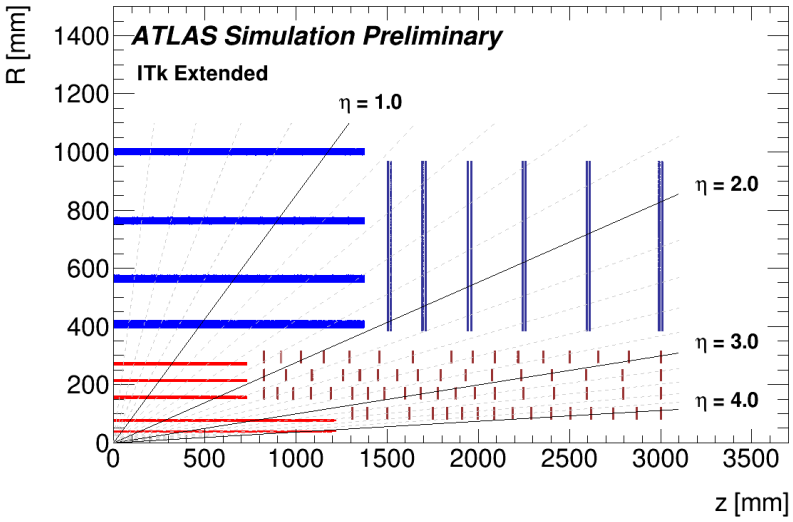

(a) Extended layout

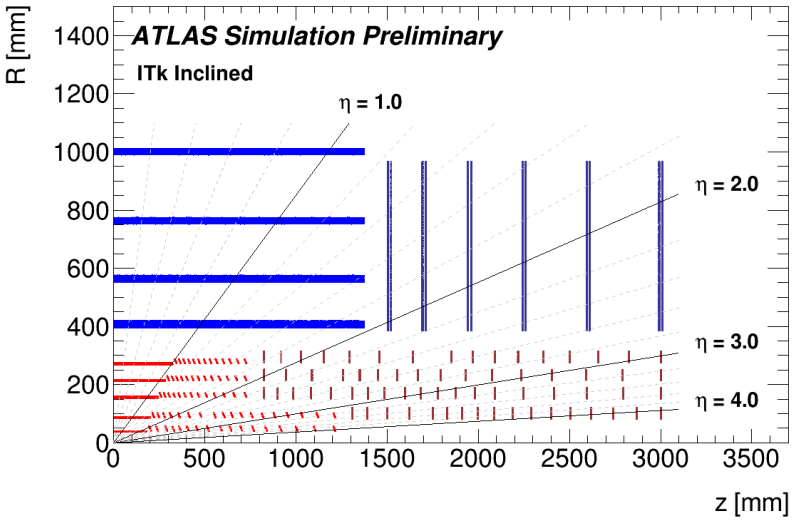

(b) Inclined layout

Figure 1: Diagrams showing simulated energy deposits in active layers for two candidate ITk layouts with either an (a) "Extended" or (b) "Inclined" Pixel barrel, shown in the R–z plane. The Pixel tracker is in red, while the Strip tracker is blue.

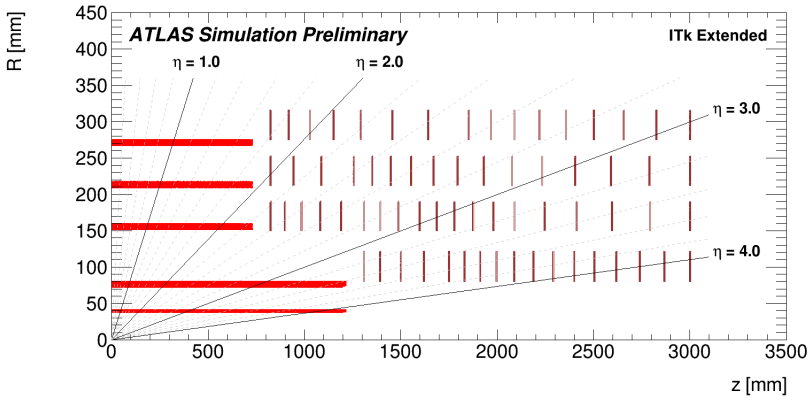

(a) Extended layout

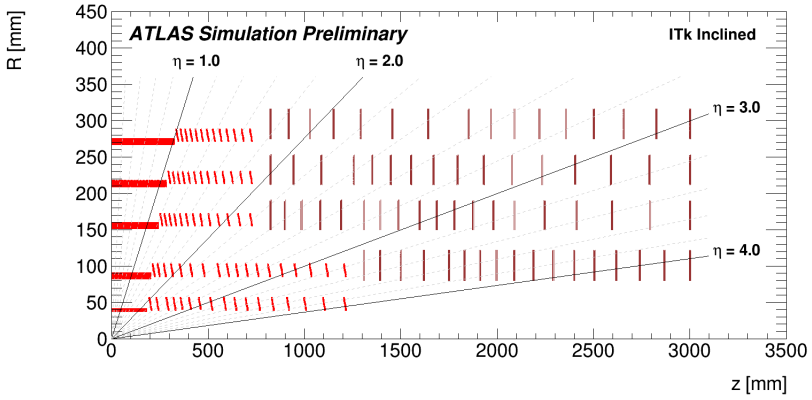

(b) Inclined layout

Figure 2: Diagrams showing simulated energy deposits in active layers for the two candidate layouts zoomed in on the Pixel barrel, which either has (a) two "Extended" innermost layers or (b) "Inclined" modules in all layers.

length can be used to reduce the number of possible cluster combinations in the track-finding procedure, though at the cost of each track crossing more material.

The "Inclined" layout has a Pixel barrel in which all five layers have some sensors that are inclined at an oblique angle with respect to horizontal. In the innermost 2 barrel layers, the inclined sensors are densely arranged to provide uniform coverage with either 1, 2, or 3 clusters per layer. Compared to the Extended layout, this results in many more clusters close to the primary vertex, but with much shorter length. The number of clusters per track is higher and each track crosses less material. In the outer barrel layers, the inclined sensors are arranged to produce 1 cluster per layer, but at a roughly perpendicular incidence angle. This results in a roughly equivalent performance to a conventional "flat" barrel layer, but with less silicon needed for uniform coverage.

Tables 1 - 4 indicate the location and size of the barrel staves and endcap rings or disks for the Pixel and Strip subdetectors. For the Inclined layout, the interval in $|z|$ instrumented with inclined modules in the barrel is also given.

Extended (Inclined) layout

Layer	Module type	Half Stave Length [mm]	Radius [mm]	Inclined module $\|z\|$ positions [mm] (Inclined layout only)
0	2×1	1218 (1250)	39	193.8 – 1206.9
1	2×2	1218 (1250)	75 (85)	210.4 – 1206.5
2	2×2	731 (780)	155	250.1 – 719.6
3	2×2	731 (780)	213	291.7 – 719.5
4	2×2	731 (780)	271	332.7 – 719.4

Table 1: Module type, stave half length and radii of the five Pixel barrel layers in the ITk layouts under study. Where the layouts differ, the value corresponding to the "Inclined" layout is given in parentheses. For the Inclined layout, the locations of the first and last inclined module in $|z|$ along the stave are also given. The module type is defined in Section 3.1.

Layer	Module type	Radius [mm]	Module $\|z\|$ positions [mm]
0	2×2	80	1308 - 3000
1	2×2	150	823 - 3000
2	2×2	212	823 - 3000
3	2×2	275	823 - 3000

Table 2: Module type and radius of the Pixel endcap rings in both layouts, as well as the range of module $|z|$ positions. The module type is defined in Section 3.1.

Layer	Half Stave Length [mm]	Radius [mm]
0	1371.83	405
1	1371.83	562
2	1371.83	762
3	1371.83	1000

Table 3: Half stave length and radius of the four Strip barrel layers for the ITk layouts under study.

Disk	$\|z\|$ [mm]	R [mm]
0	1512	384.5 – 967.8
1	1702	384.5 – 967.8
2	1952	384.5 – 967.8
3	2252	384.5 – 967.8
4	2602	384.5 – 967.8
5	3000	384.5 – 967.8

Table 4: Location in $|z|$ and instrumented interval in the radial coordinate R of the six Strip endcap petal disks per side

3. Detector simulation

3.1. Modeling and material

To evaluate the ITk performance, the tracker has been simulated [10] using GEANT4 [11] for both of the layouts described in Section 2.2. All Pixel sensors are modeled as planar n-in-n sensors, with a 150 μm sensor thickness and $50 \times 50\,\mu\text{m}^2$ pixel size. The FE-I4 readout chips [12] are emulated in the simulation, with time-walk simulation and compensation turned off. The charge threshold for the readout chips is set to 600e. The sensors are reverse biased with a voltage of 150 V. Modules comprising 1×1, 1×2, 2×1, or 2×2 readout chips in length and width are used, where one Pixel readout chip has dimensions of 20.0×16.8 mm in length and width, respectively. The innermost barrel layer of both layouts uses modules of 2 chips in length and 1 chip in width, while the four following layers use wider 2×2 chip modules. The modules in the "flat" portions of the Pixel barrel layers have a tilt of -14° with respect to the tangential direction for both layouts. For the Inclined layout, the inclined portions of the Pixel barrel layers consist of single chip modules in the innermost layer and 2 chip wide, single chip length modules in the following layers. The inclined modules are tilted at a polar angle of 56 degrees with respect to the beam. In the inclined sections of staves, adjacent modules in ϕ are shifted along z with respect to each other. This allows them to be staggered along ϕ such that their lower portions at smaller radii overlap. The endcap rings use modules of 2×2 chips in all four layers.

The Strip tracker is modeled using 320 μm thick n-in-p sensors. The inner (outer) two barrel layers have strips of length 24.1 mm (48.2 mm), while in the endcaps the strip length varies between 19–60 mm depending on the radius. Each barrel layer (endcap disk) consists of pairs of detectors positioned back-to-back and with a stereo angle of ±26 mrad (±20 mrad) with respect to the beam (radial) direction, resulting in a total stereo angle of 52 mrad (40 mrad). The barrel strips have a pitch of 75.5 μm, while the pitch in the endcaps is similar but varies with the radius. Improving on the earlier layouts studied in the LoI and Scoping Document, the 6 Strip discs per endcap are modeled as consisting of 32 petals each. No defects are modeled in either the Pixel nor Strip trackers.

The simulated silicon hits in the R–z plane for the layouts under study are shown in Figures 1–2, demonstrating the location of the sensors. The position of simulated detector material in this plane is illustrated in Figure 3. The structure of the material along ϕ is fully modeled in the simulation, while the passive material from supports and services is smeared across the staves, petal rings, and shells of the ITk. In addition to the tracker material, the beam pipe as well as supports and services for the Pixel and Strip systems are visible. Figure 4 depicts the total amount of material traversed as a function of $|\eta|$, broken down into individual components. The amount of material due to the readout chips has been estimated with a safety margin of up to a factor of 2.

3.2. Simulated samples

A variety of simulated samples of single particles are used for the studies in this note. These include muons simulated with fixed transverse momenta with $|\eta| < 4.2$, neutral pions with a continuous momentum spectrum and $|\eta| < 5.5$, and τ leptons with a flat p_{T} spectrum and $|\eta| < 5.5$, as indicated in Table 5. In addition, simulated pp collision events at $\sqrt{s} = 14$ TeV are used, as presented in Table 6. Minimum-bias interactions are generated using Pythia 8 [13] with the A2 tuned parameter set [14] and the MSTW2008LO parton distribution functions [15]. Events with top quark pairs, $t\bar{t}$, are generated using

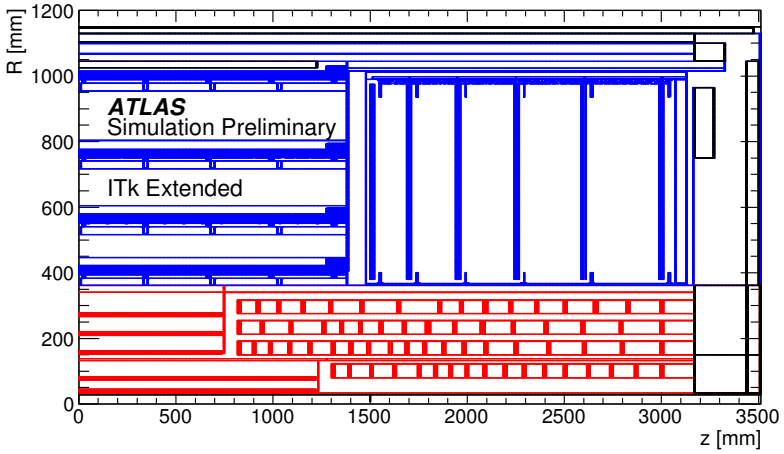

(a) Extended layout

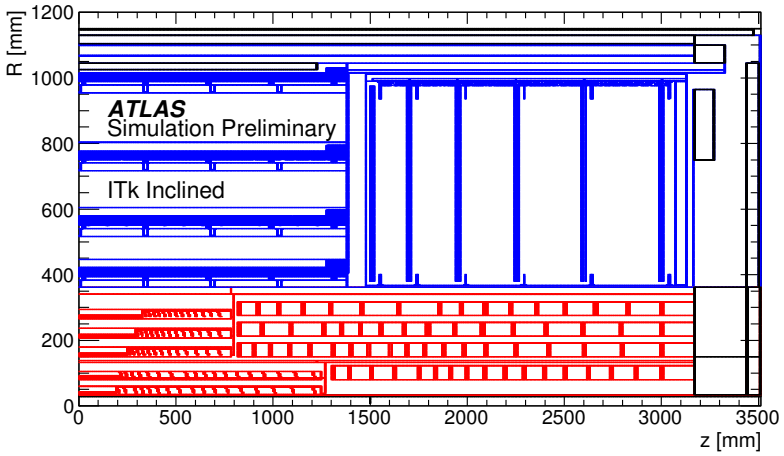

(b) Inclined layout

Figure 3: Locations of simulated detector material in the R–z plane for one quadrant of a simulated ITk with either an (a) Extended or (b) Inclined Pixel barrel. The Pixel system is indicated in red, the Strip system in blue, and other components are in black.

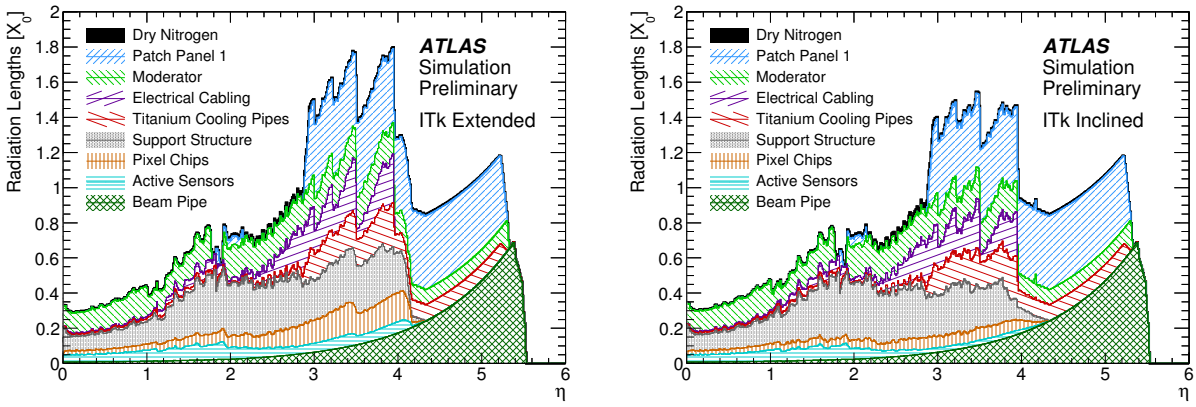

(a) Extended (b) Inclined

Figure 4: Composition of simulated detector material in radiation lengths, shown as a function of η for a simulated ITk with either an (a) Extended or (b) Inclined Pixel barrel.

Species	p_T or E interval	p_T or E distribution	μ	Sim. Events
$\mu^{\pm}$	p_{T} =1, 2, 5, 10, 100 GeV	fixed	0	50000
π^0	$0.2 < E < 2000$GeV	logarithmic	0, 190–210	50000
$\tau^{\pm}$ (3-prong hadronic)	$2 < p_{\mathrm{T}} < 2000$GeV	flat	0, 190–210	50000

Table 5: Single-particle samples with variable p_{T} used.

Process	Generator	μ	Sim. Events
$t\bar{t}$ (semilepton+dilepton)	Powheg+Pythia6	0, 190–210	50000

Table 6: Collision samples used for the studies presented in this note.

Powheg-Box [16–18] and showered using Pythia 6 [19] with the Perugia2011C tuned parameter set. At least one of the top quarks is required to decay leptonically.

To reflect the conditions expected during HL-LHC data taking [3], the simulated collision events are overlaid with minimum-bias events corresponding to $190 < \mu < 210$ proton–proton interactions per bunch crossing, hereafter denoted $\langle\mu\rangle = 200$. To study the dependence of the reconstruction performance on the amount of pileup activity, an additional set of samples without any pileup activity was produced.

4. Track reconstruction and selection

4.1. Reconstruction algorithm

The track reconstruction algorithm used for these studies employs an iterative approach [20] and is still in the process of being optimised to fully exploit the current layouts. Clusters are formed from individual silicon hits, and a Lorentz angle correction accounts for the charge drift induced by the solenoidal magnetic field in the ITk.

The current version of the ITk track reconstruction estimates the cluster position as the geometric centre of the cluster. It is expected that weighting by the charge ionized in each pixel would improve the precision on the cluster position by 10–20% for both the Extended and Inclined layouts. For the long clusters in the Extended layout, the cluster length may also offer an improved measurement of the track θ coordinate. In Run 2 data analysis, a neural network is used to identify merged clusters, which have contributions from multiple charged particles [21], but this is not currently employed for the ITk track reconstruction. Instead its performance is emulated by assuming a probability for a cluster to be identified as merged and modeling this using the truth energy deposits.

Since the reconstruction procedure is not yet optimised to fully exploit the features of the candidate layouts, the performance results derived can be interpreted as conservative estimates. The performance of the Inclined layout is generally shown as being representative of the approximate performance of the two layouts. Until this optimization is performed, no definitive conclusions about the relative performance of the two layouts should be drawn.

From the clusters, space-points are constructed with each consisting of either one Pixel cluster or two paired Strip clusters. Space-point triplet combinations – hereafter referred to as "seeds" – are formed and used to seed the combinatorial Kalman filter [22]. In the first iteration, these are required to all come from the Strip detector. In subsequent iterations, track seeds with all three space-points from the Pixel detector are used. From the seeds, "roads" are built to identify additional clusters that can be attached to the seeds to form track candidates.

Following this stage of the track reconstruction, an ambiguity solving step is performed on the resulting track candidates, with the aim of rejecting incomplete and duplicate tracks, resolving situations with shared clusters between several tracks, and removing fake tracks. This is achieved by scoring the track candidates based on the presence or absence of hits when crossing the sensor layers. The procedure is repeated iteratively, attributing shared clusters to the higher scoring track candidate, and refitting all the candidates, to obtain the final set of tracks. Both the pattern recognition and ambiguity solving steps have been adapted to take into account the effects of bremsstrahlung to improve electron track reconstruction.

A single reconstruction pass is performed for the full pseudorapidity range covered by the track reconstruction, $|\eta| < 4.0$. To account for the different number of detector modules crossed by particles depending on their direction of flight (see Figure 1), the requirements applied on the number of clusters, holes, and kinematic quantities during the track formation and ambiguity solving depend on the pseudorapidity of the seed or track candidate as described in Table 7. Here a hole is a case where a cluster in a layer of the Pixel or Strip tracker is expected for a track, but is not found. Additional tuning of the requirements is expected to further improve performance in the future. The requirements used in the reconstruction for the two layouts under study differ slightly. In the case of the Inclined layout, the higher expected number of Pixel clusters in the forward region is accounted for. For the Extended layout, requirements are placed

Extended (Inclined) layout

Requirement	Pseudorapidity interval		
	$\lvert\eta\rvert < 2.7$	$2.7 < \lvert\eta\rvert < 3.4$	$3.4 < \lvert\eta\rvert < 4.0$
Pixel+Strip clusters	≥ 9	$\geq 7(9)$	$\geq 6(9)$
Pixel clusters	≥ 1	≥ 1	≥ 1
Holes	< 3	< 3	< 3
Pixel holes	< 2	< 2	< 2
Strip holes	< 3	< 3	< 3
p_T [MeV]	> 900	> 400	> 400
$\lvert d_0\rvert$	≤ 2 mm	≤ 10 mm	≤ 10 mm
$\lvert z_0\rvert$	≤ 25 cm	≤ 25 cm	≤ 25 cm

Table 7: Set of requirements applied during the track reconstruction depending on the pseudorapidity interval for the Extended (Inclined) layout, with the only difference for the Inclined layout being 9 clusters from the Pixel and Strip detectors (given in parentheses) required for the Inclined layout at all pseudorapidities.

on the properties of the clusters, such as the minimum length, shape, and whether there is a cluster in the innermost Pixel layer.

5. Tracking performance

5.1. Track properties

The mean number of clusters per track as a function of η for single muons with $p_{\mathrm{T}} = 10$ GeV for the Extended and Inclined layouts is shown in Figure 5. Each is shown for the Pixel tracker only, the Strip tracker only, and Pixel and Strip together. At least 13 silicon clusters are achieved across most of the central pseudorapidity acceptance of the detector. The mean number of clusters is increased by the overlaps between adjacent modules.

Detector defects are not implemented in the simulation. Thus any holes are due to gaps in the acceptance from insufficient module overlap, the thresholds applied in the digitization modeling of FE-I4 readout chips with thick sensors, or due to pattern recognition mistakes. The number of holes per track, which reflect the sum of both effects, is below 0.1. Most tracks have no holes.

5.2. Reconstruction efficiency, secondaries, and fakes

A charged truth particle is defined as a stable, charged, primary particle, thus excluding secondaries from hadronic interactions. A truth particle is assigned a score, termed "matching probability", whether it matches to a given reconstructed track, and vice versa, based on the fraction of clusters on the reconstructed track in each sub-detector that was produced by the primary truth particle. A "match" is defined as the case where the matching probability exceeds 0.5. The track reconstruction efficiency is defined as the fraction of truth particles that matches to a reconstructed track. It can be expressed as a conditional probability: efficiency = P(reconstructed track | truth particle). The truth particles considered have $p_{\mathrm{T}} > 1$ GeV and lie within the tracking acceptance of $|\eta| < 4.0$.

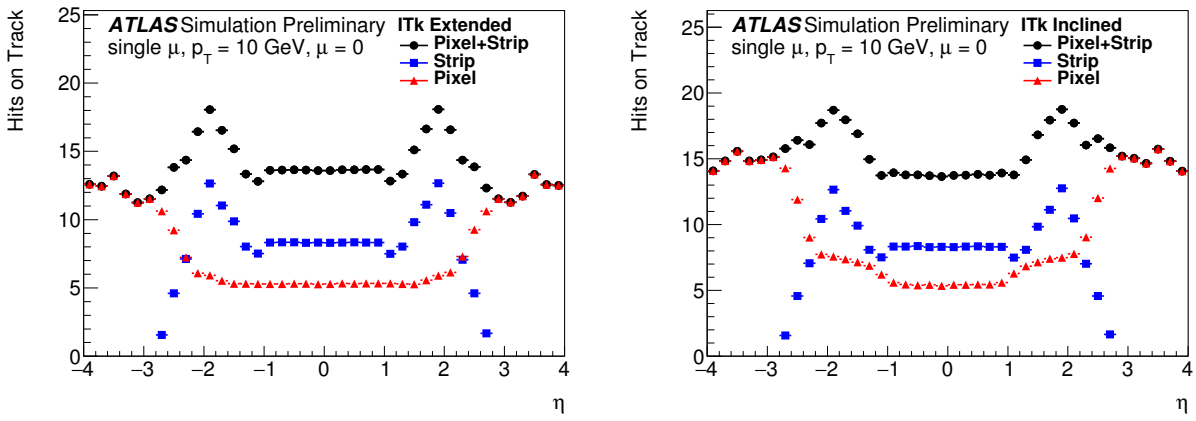

(a) Extended layout

(b) Inclined layout

Figure 5: Mean number of clusters per track as a function of η for single muons with $p_{\mathrm{T}} = 10$ GeV for the (a) Extended and (b) Inclined layouts. The error bar shows the uncertainty on the mean.

Figure 6(a) shows the efficiency to reconstruct tracks of particles with various p_{T} and η in $t\bar{t}$ events with $\langle\mu\rangle$=200 pileup, with the Inclined layout only. A reconstruction efficiency of 90% in the central region, and at least 80% in almost the entire pseudorapidity range $|\eta| < 4.0$, is attained. The inefficiency observed is largely due to the rate of hadronic interactions with the detector material, as the single hit efficiency of the track reconstruction itself is close to 99%.

The ratio of the numbers of reconstructed tracks and charged truth particles, $N_{\mathrm{reco}}/N_{\mathrm{true}}$, where no reconstructed–true matching criteria are applied, is shown in Figure 6(b). For $N_{\mathrm{reco}}/N_{\mathrm{true}}$, both the truth particle and the reconstructed track are required to satisfy $p_{\mathrm{T}} > 1$ GeV. This is done to avoid potential enhancements from upward fluctuations of the reconstructed track p_{T} for soft truth particles, especially due to the coarse p_{T} resolution in the forward region. The measured ratio exhibits no large enhancements and has a similar shape to the efficiency curve. This demonstrates that the number of additional secondaries from hadronic interactions of the incident particles with the detector material as well as the number of falsely reconstructed tracks with no associated truth particle are not large. Together the efficiency and the ratio $N_{\mathrm{reco}}/N_{\mathrm{true}}$ imply a strong correspondence between the true particles and the tracks that are reconstructed.

The fake rate is defined as the fraction of reconstructed tracks that does not match to a truth particle. It can be expressed as a conditional probability: fake rate = P(no truth track | reconstructed track). For the Inclined layout, the fake rate is below 0.001 in the region $|\eta| < 3.5$.

5.3. Parameter resolutions

The trajectory of each track is characterized using five parameters determined at the point of closest approach to the beam axis:

- q/p: the ratio of the charge to the momentum
- ϕ_0: the azimuthal angle

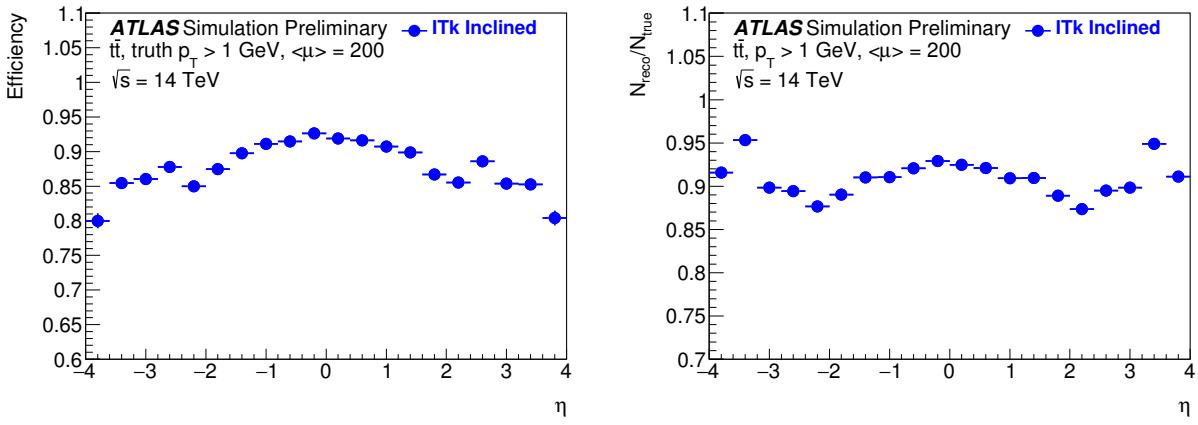

(a) Reconstruction efficiency

(b) Ratio of numbers of reconstructed and truth tracks

Figure 6: (a) Track reconstruction efficiency, where criteria to match truth particles and reconstructed tracks are applied as indicated in the definition of efficiency given in the body, and (b) ratio of numbers of reconstructed tracks and truth particles, where no such matching criteria are used. Each is shown as a function of η for tracks in $t\bar{t}$ events with $\langle\mu\rangle = 200$ pileup.

- θ_0: the polar angle
- d_0: the signed distance to the beam axis, where the sign is positive when $\phi - \phi_0 = \frac{\pi}{2} \mod 2\pi$
- z_0: z coordinate of the track

The resolutions on the track parameters are determined using an iterative procedure in which the RMS of a parameter is determined, outliers beyond 3σ of the mean are removed, and the RMS is recalculated. This is repeated until a stable value for the RMS is found, which is assigned as the resolution.

Figure 7 shows the resolutions on the transverse and longitudinal impact parameters, $\sigma(d_0)$ and $\sigma(z_0)$, the resolutions on the azimuthal and polar angles, $\sigma(\phi_0)$ and $\sigma(\theta_0)$, as well as the relative resolution on the curvature, $p_T\,\sigma(1/p_T)$. These are shown for single muons with various p_T using the Inclined layout.

The resolutions of low-energy particles are generally dominated by multiple scattering, whose contribution falls rapidly with energy. At high p_T the resolutions are dominated by the intrinsic detector resolution, which is determined by the pitch of the sensor pixels and strips, as well the positions and orientations of the modules. The resolutions at $p_\mathrm{T} = 10$ GeV receive contributions from both multiple scattering and the intrinsic resolution of the detector. For 10 GeV tracks with the Inclined layout, the resolutions $\sigma(d_0)$ and $\sigma(z_0)$ are better than 35 μm and 300 μm respectively in the region $|\eta| < 3.5$. The ITk impact parameter resolutions at $|\eta| = 3.5$ are comparable to or better than those of the Run 2 Inner Detector [23] at $|\eta| = 2.5$. This demonstrates the potential for the physics program to be extended to use tracking, vertexing, b-tagging, and pileup jet rejection, in the forward region.

For 10 GeV tracks at $|\eta| = 4.0$, somewhat worse impact parameter resolutions of 50 μm in d_0 and 450 μm in z_0 are achieved. For 100 GeV tracks, only the intrinsic resolution remains, resulting in lower corresponding impact parameter resolutions of 35 μm and 200 μm.

The relative resolution on the curvature, $p_T\,\sigma(1/p_T)$, is about 0.87% at $\eta = 0$. This is significantly better than that of the Run 2 Inner Detector [23]. At $|\eta| = 4.0$ the curvature resolution – or equivalently transverse momentum resolution – degrades due to the shorter lever arm with respect to the magnetic field. However forward particles of a given energy have a much softer p_{T} spectrum due to the small transverse component with respect to the beam axis. A relative curvature resolution of 13% (40%) is retained for muons with $p_{\mathrm{T}} = 1$ GeV (10 GeV) in the forward region.

5.4. Dense environments

A key requirement of the ITk is the ability to successfully reconstruct tracks in dense environments, for example close to a jet axis or due to hadronically decaying, highly-boosted τ leptons. The proper identification of merged pixel clusters is crucial for the track reconstruction performance in these dense environments [24]. The ITk Pixel front-end chip will, similarly to that of the Run 2 Pixel detector, provide information about the deposited charge in each pixel. The merged cluster identification capabilities with a neural network are therefore emulated based on truth information. The performance observed using this emulated pixel cluster splitting is slightly better than the Run 2 performance, with a relative difference of less than 7% for the process and kinematic region studied.

The 3-prong hadronic decays of single τ leptons without pileup were studied using the corresponding samples in Table 5. In Figure 8, the efficiency to reconstruct tracks from all three charged pions in these decays is depicted as a function of the τ lepton transverse momentum, for three ranges of pseudorapidity. Each truth pion of the τ lepton decay is required to be matched to a distinct reconstructed track with a matching probability greater than 0.5, based on the clusters of the track. The tracks are required to satisfy the criteria given in Table 7. For a 1 TeV τ lepton with $|\eta| < 1.0$, the efficiency is only 9% lower than the maximum efficiency, which is attained at about 300 GeV.

5.5. Photon conversions

For photons, the amount of material traversed increases the probability for a photon to convert into an electron–positron pair within the acceptance. In addition, the choice of the layout affects the efficiency to reconstruct the photons that have converted. A conversion track-finding algorithm has been developed for the ITk. This new algorithm runs after the usual track-finding algorithm, and takes the unused clusters to build tracks with loosened requirements, such as allowing tracks to have fewer clusters, not to point back to the primary vertex, and to begin at a larger radius than a standard track (see Figure 8). The reconstructed conversions may involve either a single track or two tracks.

The cumulative probability for photon conversion as a function of radius obtained using a sample of single π^0 with a logarithmic energy spectrum spanning the range 0.2 GeV $< E <$ 2 TeV with $\langle\mu\rangle = 200$ pileup (see Table 5) is shown in Figure 9. The probability for a photon in the central barrel region $|\eta| < 1.0$ (barrel–endcap transition region $1.52 < |\eta| < 2.37$) to convert within a radius of 1.2 m from the interaction point is approximately 22% (38%) for both the Extended and Inclined layouts. In the barrel (endcap) region, the Inclined (Extended) layout has a slightly higher probability to convert as it has more material in this $|\eta|$ slice.

A dedicated algorithm, which takes into account the massless nature of photon, is used to identify a pair of tracks or a single track consistent with a photon conversion and determine the conversion vertex. Clusters in the electromagnetic calorimeter matched to a track associated with a conversion vertex are

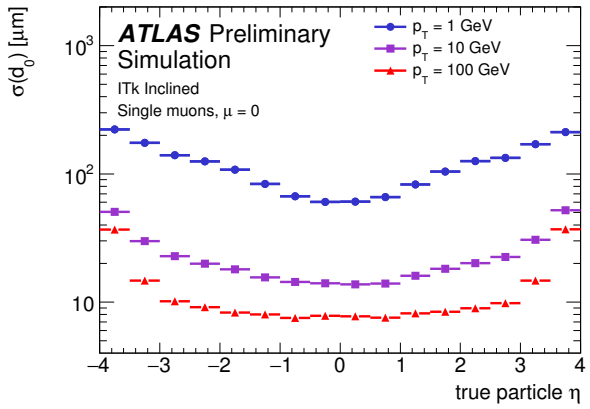

(a) $\sigma(d_0)$

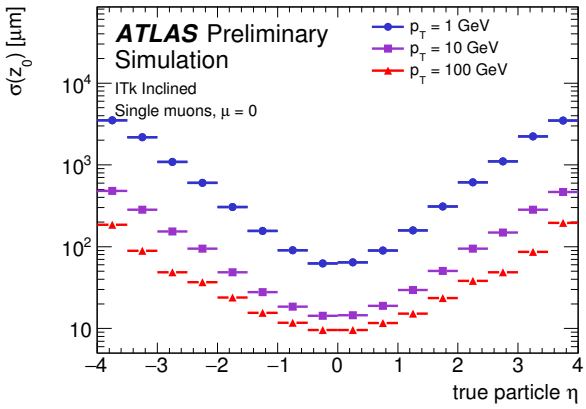

(b) $\sigma(z_0)$

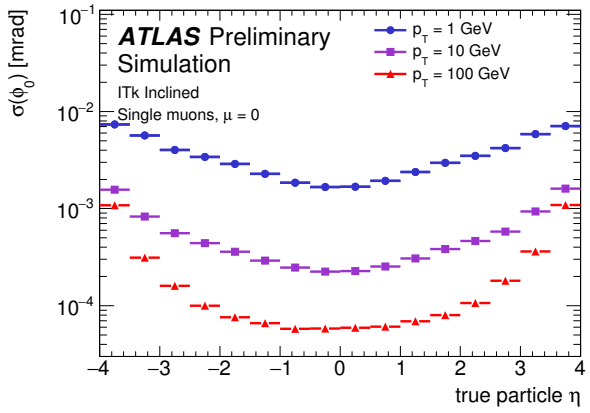

(c) $\sigma(\phi_0)$

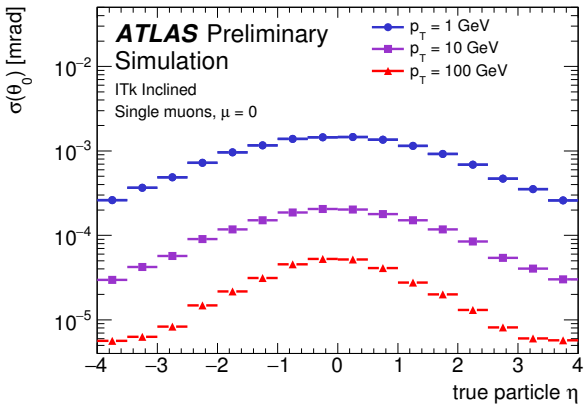

(d) $\sigma(\theta_0)$

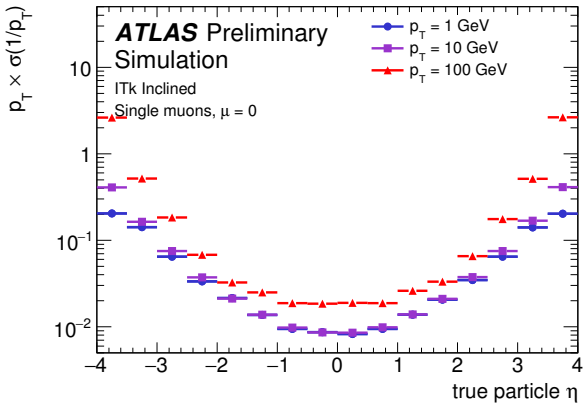

(e) $p_T\,\sigma(1/p_T)$

Figure 7: Resolutions on track parameters, (a) $\sigma(d_0)$, (b) $\sigma(z_0)$, (c) $\sigma(\phi_0)$, and (d) $\sigma(\theta_0)$, as well as (e) $p_T\,\sigma(1/p_T)$. These are shown as a function of true track η, for single muons with p_{T} of 1, 10, or 100 GeV, using the Inclined layout.

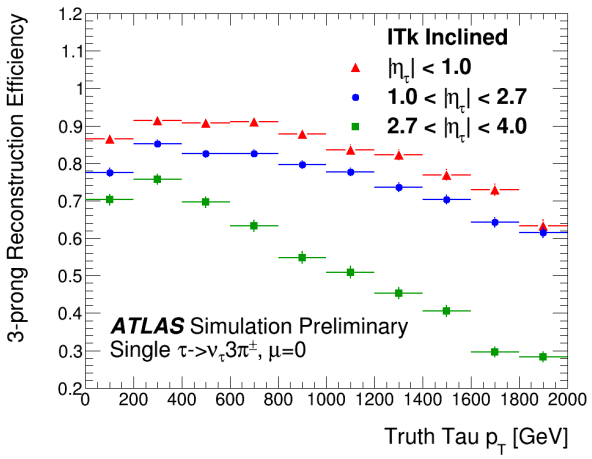

Figure 8: Efficiency to reconstruct tracks from all three charged pions in a 3-prong τ decay, as a function of the τ lepton p_{T}, in the central region $|\eta| < 1.0$, barrel–endcap transition region $1.0 < |\eta| < 2.7$, and forward region $2.7 < |\eta| < 4.0$. Each truth pion of the τ lepton decay is required to be matched to a distinct reconstructed track with a probability greater than 0.5, based on the clusters of the track. The tracks are required to satisfy the criteria given in Table 7.

Variable	Requirement
Pixel+Strip clusters	≥ 6
Pixel clusters	≥ 0
Holes	0
p_T [MeV]	> 900
$\lvert\eta\rvert$	≤ 2.7
$\lvert d_0\rvert$	≤ 10 mm
$\lvert z_0\rvert$	≤ 125 mm

Table 8: Set of requirements applied during the dedicated conversion track-finding reconstruction pass.

reconstructed as converted photon candidates. The distributions of the vertex radius for reconstructed and true photon conversions, and their ratio which is the conversion reconstruction efficiency, are shown in Figure 10. The efficiency is higher for photons that convert earlier in the detetor. Both the Extended and Inclined layouts reconstruct conversions of photons from π^0 decays that have $p_{\mathrm{T}} > 20$ GeV and $|\eta|$ <2.5 with an overall efficiency of about 35%.

6. Conclusions

The Inner Tracker is an all-silicon replacement for the current ATLAS tracker that is planned for Phase II. It is being designed to cope with the challenging environment at the High-Luminosity LHC. Good tracking performance has been achieved using two candidate ITk layouts, having either an Extended or Inclined Pixel barrel. Both layouts have been modeled using the full simulation and perform better than the current Run 2 detector despite the $\langle\mu\rangle$=200 pileup conditions.

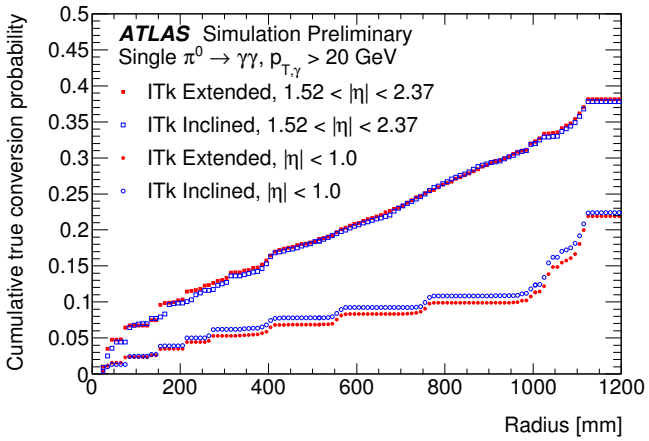

Figure 9: The cumulative probability of conversion as a function of radius for the Extended and Inclined layouts. It is shown separately for photons in the central barrel region $|\eta| < 1.0$ and the barrel–endcap transition region $1.52 < |\eta| < 2.37$. The results are derived using $\pi^0 \rightarrow \gamma\gamma$.

For the Inclined layout, the ITk is able to reconstruct tracks in $t\bar{t}$ events with $\langle\mu\rangle = 200$ pileup with an efficiency of at least 80% in the region $|\eta| < 4.0$, including around 90% in the central region. The track reconstruction efficiency is high even in dense environments like hadronic decays of boosted τ leptons. The fake rate is below 0.001 in the $|\eta| < 3.5$ region. For single muons with $p_{\mathrm{T}} = 10$ GeV, the resolutions $\sigma(d_0)$ and $\sigma(z_0)$ are better than 35 μm and 300 μm respectively in the region $|\eta| < 3.5$. The performance at $|\eta| = 3.5$ is comparable to or superior than the Run 2 performance at $|\eta| = 2.5$, demonstrating the potential to extend the tracking-based physics program out to forward pseudorapidities. The relative resolution on the curvature, $p_T\,\sigma(1/p_T)$, at $\eta = 0$ is about 0.87%, which is significantly better than that in Run 2.

Detailed comparisons between the Extended and Inclined layouts are not possible with the current tracking reconstruction, whose optimization is layout specific. Neither the layouts nor the track reconstruction algorithms have been optimized. Therefore no conclusions about the ultimate performance of either layout, nor which Pixel barrel design performs better, can be drawn at present.

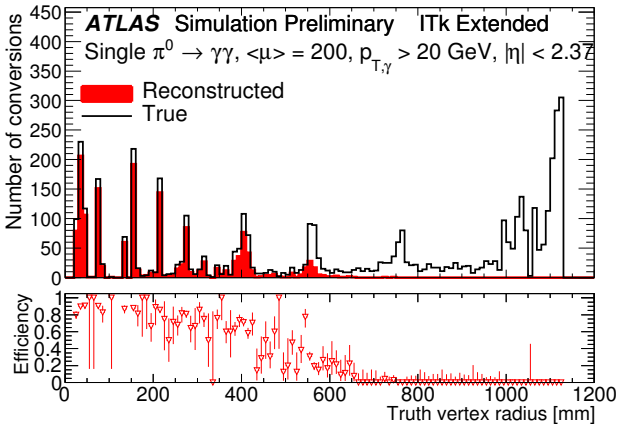

(a) Extended

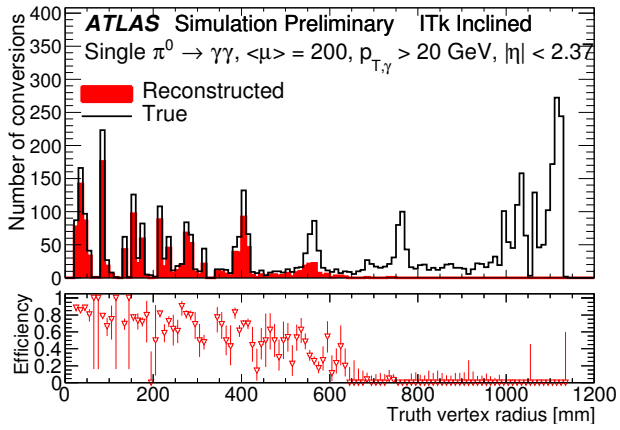

(b) Inclined

Figure 10: Distributions of true conversion vertex radius for reconstructed (red) and true (black) converted photons with $|\eta|$ <2.37 (top panel). Their bin-wise ratio is the conversion reconstruction efficiency as a function of true radius (bottom panel). These are shown for the (a) Extended and (b) Inclined layouts. The results are derived using $\pi^0 \to \gamma\gamma$.

References

[1] *HL-LHC High Luminosity Large Hadron Collider: The HL-LHC project*, (Accessed 2016), URL: http://hilumilhc.web.cern.ch/about/hl-lhc-project.

[2] ATLAS Collaboration, *Letter of Intent for the Phase-II Upgrade of the ATLAS Experiment*, CERN-LHCC-2012-022, LHCC-I-023 (2012), URL: https://cds.cern.ch/record/1502664.

[3] ATLAS Collaboration, *ATLAS Phase-II Upgrade Scoping Document*, CERN-LHCC-2015-020. LHCC-G-166 (2015), URL: https://cds.cern.ch/record/2055248.

[4] *ECFA High Luminosity LHC Experiments Workshop: Physics and Technology Challenges. 94th Plenary ECFA meeting*, ECFA-13-284 (2013), URL: https://cds.cern.ch/record/1631032.

[5] *ECFA High Luminosity LHC Experiments Workshop: Physics and Technology Developments Summary. 96th Plenary ECFA meeting*, ECFA-15-289 (2015), URL: https://cds.cern.ch/record/1983664.

[6] ATLAS Collaboration, *Projections for measurements of Higgs boson signal strengths and coupling parameters with the ATLAS detector at a HL-LHC*, ATL-PHYS-PUB-2014-016 (2014), URL: https://cds.cern.ch/record/1956710.

[7] ATLAS Collaboration, *Prospects for New Physics in Higgs Couplings Studies with the ATLAS Detector at the HL-LHC*, ATL-PHYS-PUB-2014-017 (2014), URL: https://cds.cern.ch/record/1956711.

[8] ATLAS Collaboration, *Studies of Vector Boson Scattering And Triboson Production with an Upgraded ATLAS Detector at a High-Luminosity LHC*, ATL-PHYS-PUB-2013-006 (2013), URL: https://cds.cern.ch/record/1558703.

[9] ATLAS Collaboration, *Prospect for a search for direct pair production of a chargino and a neutralino decaying via a W boson and the lightest Higgs boson in final states with one lepton, two b-jets and missing transverse momentum at the high luminosity LHC with the ATLAS Detector.*, ATL-PHYS-PUB-2015-032 (2015), URL: https://cds.cern.ch/record/2038565.

[10] ATLAS Collaboration, *The ATLAS Simulation Infrastructure*, Eur. Phys. J. C **70** (2010) 823, arXiv: 1005.4568 [hep-ex].

[11] S. Agostinelli et al., *GEANT4: A simulation toolkit*, Nucl. Instrum. Meth. A **506** (2003) 250–303.

[12] M. Garcia-Sciveres et al., *The FE-I4 pixel readout integrated circuit*, Nucl. Instrum. Meth. **A636** (2011) S155–S159.

[13] T. Sjostrand, S. Mrenna and P. Z. Skands, *A Brief Introduction to PYTHIA 8.1*, Comput. Phys. Commun. **178** (2008) 852, arXiv: 0710.3820 [hep-ph].

[14] ATLAS Collaboration, *Summary of ATLAS Pythia 8 tunes*, ATL-PHYS-PUB-2012-003 (2012), URL: https://cds.cern.ch/record/1474107.

[15] A. D. Martin et al., *Parton distributions for the LHC*, Eur. Phys. J. **C63** (2009) 189–285, arXiv: 0901.0002 [hep-ph].

[16] P. Nason, *A New method for combining NLO QCD with shower Monte Carlo algorithms*, JHEP **0411** (2004) 040, arXiv: 0409146 [hep-ph].

[17] S. Frixione, P. Nason and C. Oleari,
Matching NLO QCD computations with Parton Shower simulations: the POWHEG method,
JHEP **0711** (2007) 070, arXiv: 0709.2092 [hep-ph].

[18] S. Alioli et al., *A general framework for implementing NLO calculations in shower Monte Carlo programs: the POWHEG BOX*, JHEP **06** (2010) 043, arXiv: 1002.2581 [hep-ph].

[19] T. Sjostrand, S. Mrenna and P. Z. Skands, *PYTHIA 6.4 Physics and Manual*,
JHEP **0605** (2006) 026, arXiv: 0603175.

[20] T Cornelissen et al., *Concepts, Design and Implementation of the ATLAS New Tracking (NEWT)*,
ATL-SOFT-PUB-2007-007 (2007), URL: https://cds.cern.ch/record/1020106.

[21] ATLAS Collaboration,
A neural network clustering algorithm for the ATLAS silicon pixel detector,
JINST **9** (2014) P09009, arXiv: 1406.7690 [hep-ex].

[22] R. Fruhwirth, *Application of Kalman filtering to track and vertex fitting*,
Nucl. Instrum. Meth. **A262** (1987) 444–450.

[23] ATLAS Collaboration, *ATLAS Insertable B-Layer Technical Design Report*,
CERN-LHCC-2010-013 (2010), URL: https://cds.cern.ch/record/1291633.

[24] ATLAS Collaboration, *The Optimization of ATLAS Track Reconstruction in Dense Environments*,
(2015), URL: https://cds.cern.ch/record/2002609.

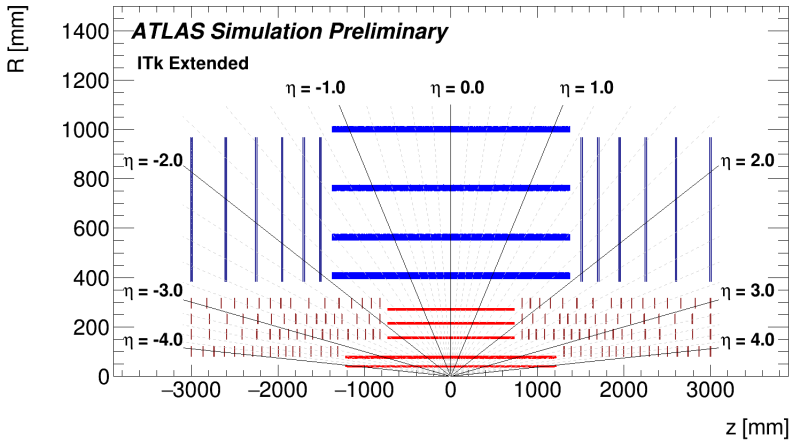

(a) Extended layout

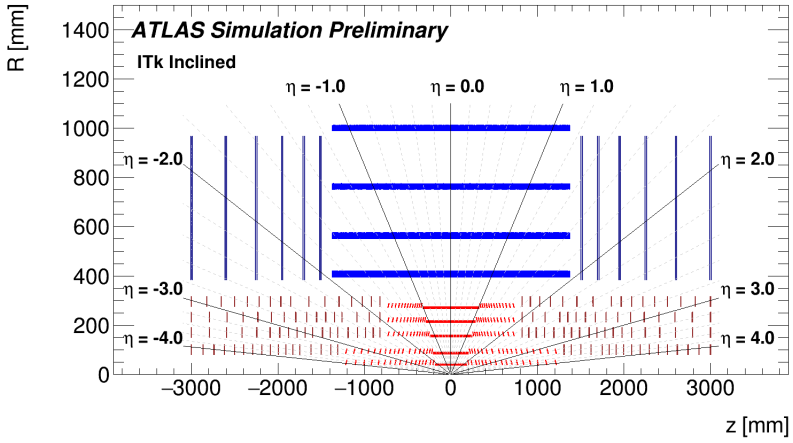

(b) Inclined layout

Figure 11: Diagrams showing simulated energy deposits in active layers for two candidate ITk layouts with either an (a) "Extended" or (b) "Inclined" Pixel barrel, shown in the R–z plane. The Pixel tracker is in red, while the Strip tracker is blue. Both positive and negative hemispheres in η are shown.

A. Appendix

A.1. Layout diagrams with positive and negative η

The same layout diagrams described in Section 2 are shown in Figs. 11–12, but with both positive and negative η hemispheres displayed.

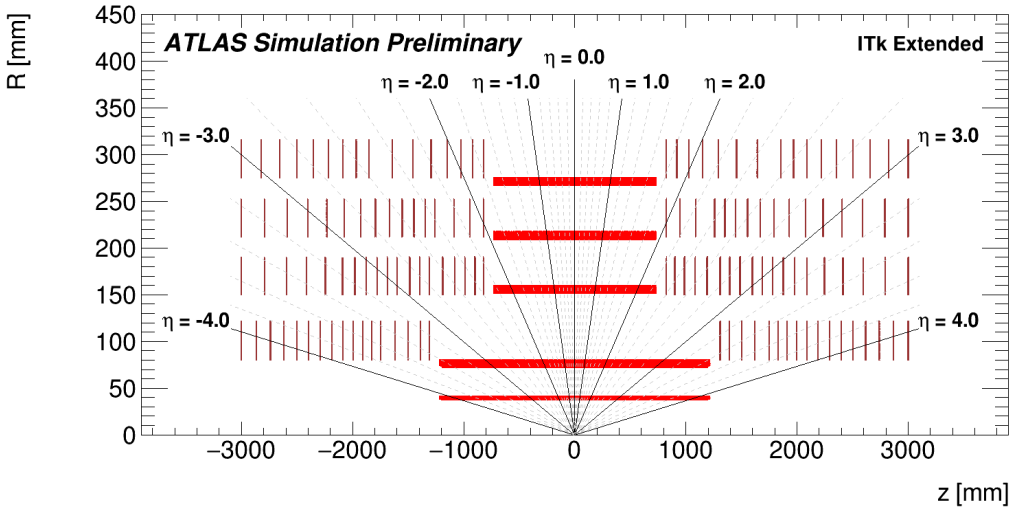

(a) Extended layout

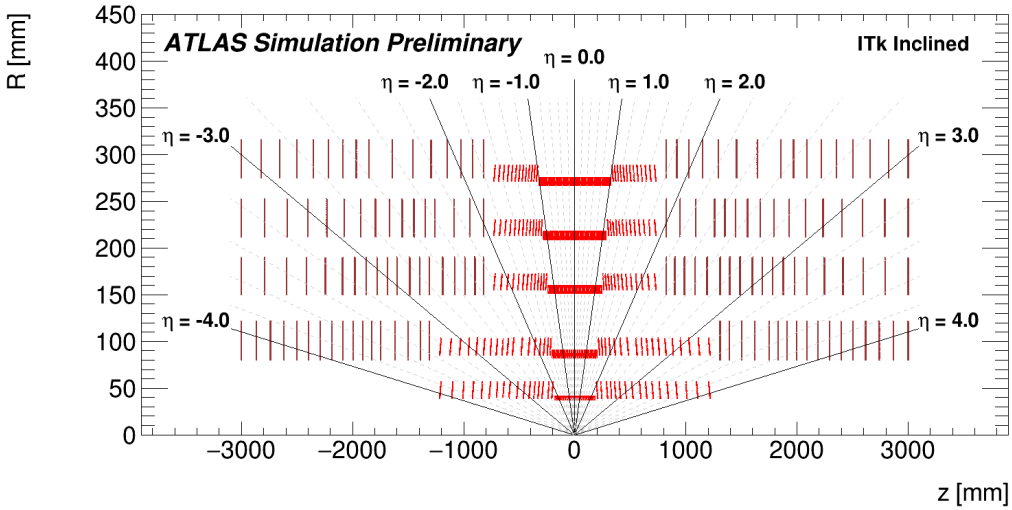

(b) Inclined layout

Figure 12: Diagrams showing simulated energy deposits in active layers for the two candidate layouts zoomed in on the Pixel barrel, which either has (a) two "Extended" innermost layers or (b) "Inclined" modules in all layers. Both positive and negative η hemispheres are shown.